Journal of the Korean Physical Society, Vol. 52, No. 2, February 2008, pp. 476∼480

Light-Emitting Characteristics of Top-Emitting Organic Light-Emitting Diodes Based on the Interfacial Electronic Feature of Cs-on-Alq_3

Jong Tae Lim, June Hee Lee, Yang Su Kim and G. Y. Yeom*
School of Advanced Materials Science and Engineering, Sungkyunkwan University, Suwon 440-746

(Received 12 November 2007)

This study used ultraviolet photoelectron spectroscopy (UPS) and X-ray photoemission spectroscopy (XPS) to examine the interfacial electronic structures of Cs deposited on tris(8-quinolinolato)aluminum (III) (Alq_3). In the valence band spectra, the low work function of Cs reduces the barrier height for electron injection (Φ_n^B) in the Cs-on-Alq_3 interfaces to 0.2 eV when a 1- $\sim$ 3-nm-thick layer of Cs is deposited on Alq_3. This decrease in Φ_n^B to 0.6 eV means more efficient electron injection than with a Φ_n^B of 0.8 eV for the pure Alq_3 layer. The XPS O 1s peak revealed a two-step interface reaction, which showed the formation of a stable radical anion for low Cs coverage ($\Theta_{Cs} \leq 0.4$ nm) and the appearance of a metallic component through the decomposition of the highly reactive Cs at higher coverage ($\Theta_{Cs} \geq 1.0$ nm). Top-emitting organic light-emitting diodes with Θ_{Cs} (1.0 nm) based on these interfacial electronic structures showed much higher device performance with a luminous efficiency of 2.0 % and a maximum luminance of 48000 cd/m^2 compared to other devices with $\Theta_{Cs} > 1.0$ nm.

PACS numbers: 81.15.J, 72.80.L
Keywords: Top emission, Organic light-emitting diodes, Cs/Au, Electronic structure, UPS, XPS

I. INTRODUCTION

Recently, there has been a great deal of interest in functional molecular organic thin films with respect to their potential use in a wide variety of optoelectronic devices, such as organic light-emitting diodes (OLEDs) [1–4], organic solar cells [5], and organic sensors [6]. Among these, OLED devices have been developed steadily for applications in flat-panel displays (FPDs) that would meet the future demands of information displays.

Operation of the above devices always involves metal / organic interfaces, and the function of these interfaces is very important [7,8]. In the interface, knowledge of the energy level alignment between the work function of the metal electrode and the highest occupied molecular orbital (HOMO) / lowest unoccupied molecular orbital (LUMO) level of the organic layer is crucial for charge injection and the device performance [7]. In addition, the electronic structure based on an interfacial chemical reaction between a metal and the organic layer can form the basis for understanding chemical processes, such as device degradation [9].

In a typical OLED, an organic layer is placed next to a metal, forming a metal / organic interface. The choice of these contacting electrodes is governed primarily by the work function relationship, *i.e.*, a high work function system for the anode and a low-work-function system for the cathode. Efficient electron injection from the cathode to an electron-transporting layer (ETL) can be achieved by inserting a low work function system between the ETL and the cathode. A low-work-function metal (Li [10], Cs [11], Mg [12], and Ca [13]), an ETL doped with a n-type conductive dopant [14], and an insulator, such as LiF [15], has been reported as a low-work-function system.

This paper reports the electronic structure of Cs-on-Alq_3 interfaces. As Cs is sequentially deposited on Alq_3 in-situ, the barrier height for electron injection (Φ_n^B) of the interfaces was investigated by using ultraviolet photoemission spectroscopy (UPS). In addition, the interfacial chemical reaction of Cs-on-Alq_3 was examined by using X-ray photoemission spectroscopy (XPS) to analyze the O 1s core-level electron density curves (EDCs). The results of the interfacial electronic structures can be useful, either for understanding the effects of a low work function metal or for monitoring the chemical processes that Alq_3 may undergo during the fabrication (or degradation) of OLEDs. The current density-voltage - luminance characteristics of the top-emitting (TE) OLEDs were also analyzed based on the interfacial electronic features of Cs-on-Alq_3.

II. EXPERIMENTS

The electronic structures of the Cs-on-Alq_3 interfaces were examined by using XPS and UPS at the 4B1 beam

*E-mail: gyyeom@skku.edu; Fax: +82-31-299-6565

line in the Pohang Accelerator Laboratory (Korea). All measurements and depositions were carried out in an ultra-high-vacuum system (UHV), which consisted of a main analysis chamber (approximately 5×10^{-10} Torr) and a sample preparation chamber (approximately 5×10^{-8} Torr). All samples used in interfacial analyses of the electronic structures were prepared in-situ by sequential thermal evaporation on a Si (100) wafer, and the sample thickness was determined using a quartz-crystal microbalance. In addition, before collecting the photoemission spectra, the absence of charging effects in the samples was confirmed by observing the reproducibility of the O 1s peak position of a 10-nm-thick Alq_3 layer. In the XPS studies, the core-level spectra of O 1s were obtained using an incident photon energy of 550 eV. For the UPS measurements, the He I (21.2 eV) line from a UV source was used. The onset of photoemission corresponding to the vacuum level at the surface of all samples was measured by negatively biasing the samples at −20 V in order to avoid changes in the work function of the detector. The incident photon energy was calibrated by measuring the Au 4f core level of a clean Au surface.

The TEOLED structure consisted of glass / Ag (150 nm) / ITO (125 nm) / 4,4',4"-tris(2-naphthylphenyl-1-phenylamino)triphenylamine (2-TNATA, 30 nm) / 4,4'-bis(N-(1-napthyl)-N-phenyl-amino)-biphenyl (NPB, 18 nm) / Alq_3 (62 nm) / Cs (3 nm (device 1), 2 nm (device 2), 1 nm (device 3) and 0 nm (device 4) / Au (20 nm) / Alq_3 (51 nm). All organic layers and metal layers were deposited by thermal evaporation. Tin-doped indium oxide (ITO) in the multi-layer anode was deposited by conventional dc sputtering followed by heat treatment. The 2-TNATA, NPB, and Alq_3 function as the hole-transporting layer (HTL), the hole-injecting layer (HIL) and the ETL (and as a green emissive layer), respectively. The emissive active area of the devices was 1.4×1.4 mm^2. Alq_3 was used as the top capping layer (refractive index: 1.7) to obtain enhanced optical transmission [16].

The current-voltage - luminance characteristics were measured using a source-measure unit (2400, Keithley Instrument Inc.) and the emission intensity of the OLEDs devices was measured by using a picoammeter (485, Keithley Instrument Inc.) to measure the photocurrent induced on the silicon photodiodes. The electroluminescent (EL) spectra of the fabricated devices were measured by using optical emission spectroscopy (OES; PCM-420, SC Tech. Inc.).

III. RESULTS AND DISCUSSION

Green TEOLEDs were fabricated with the following structure: glass / Ag (150 nm) / ITO (125 nm) / 2-TNATA (30 nm) / NPB (18 nm) / Alq_3 (62 nm) / Cs (x nm) / Au (20 nm) / Alq_3 (51 nm). Here, the multilayers of Ag / ITO and Cs / Au function as the reflective conducting anode and a semi-transparent conducting cathode (STCC), respectively. The thicknesses of the Cs layer in devices 1-4 were 3, 2, 1 and 0 nm, respectively. For devices $1 \sim 4$, the electroluminescent (EL) spectra, which was measured at normal viewing angle and at L_{1000}, showed the maximum peak at a wavelength of 515 ± 2 nm (not shown). The EL spectrum at approximately 515 nm was tuned by adjusting the macrocavity length [17]. This means that it was controlled by changing the thickness of the ITO layer comprising the multilayer anode.

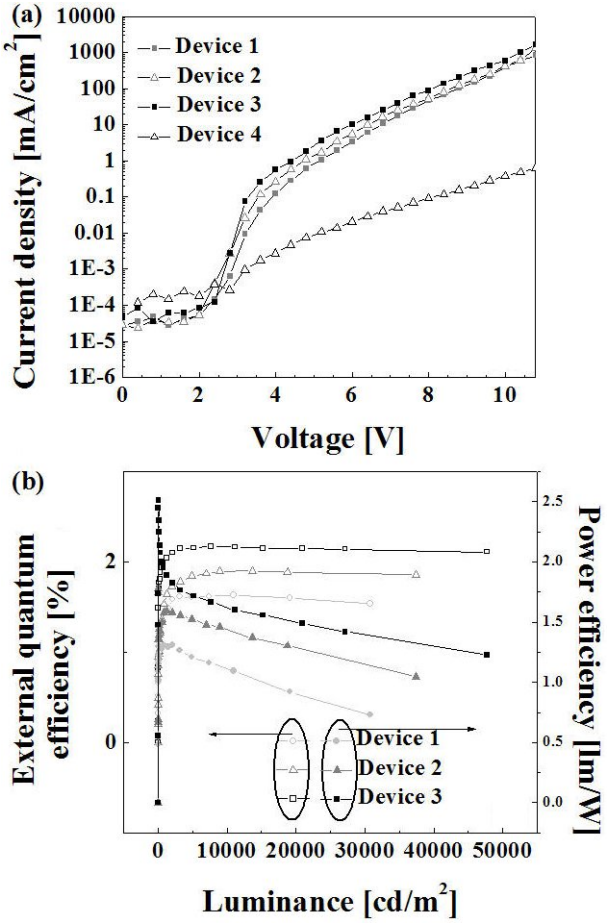

Fig. 1. (a) Current density-voltage curves and (b) external quantum efficiency - luminance - power efficiency curves for devices 1-4.

Figure 1(a) shows the current density as a function of the forward bias voltage for devices 1-4. Table 1 shows the current density-voltage - luminance characteristics for devices 1-4. At a luminance of approximately 1000 cd/m^2 (L_{1000}), the current densities of devices 1-3 were 36.2 (7.4 V), 37.9 (7.4 V) and 40.4 mA/cm^2 (7.2 V), respectively. The voltages of devices 1-3 at L_{1000} were similar, as shown in Table 1. All turn-on voltages (voltage at 0.1 cd/m^2, V_T) of devices 1-3 were 2.8 V. However, device 4, having a V_T of 7.8 V, exhibited inferior light-output characteristics compared with the other de-

Table 1. Current density-voltage - luminance characteristics for devices 1-4.

Devices	Cathode structure	η_{ext} (%)	η_{PE} (lm/W)	V_{1000} (V)	V_T (V)	L_{max} at 10.8 V (cd/m^2)
Device 1	Cs (3.0 nm) / Au (20 nm)	1.4	1.3	7.4	2.8	30,800
Device 2	Cs (2.0 nm) / Au (20 nm)	1.6	1.6	7.4	2.8	37,400
Device 3	Cs (1.0 nm) / Au (20 nm)	2.0	1.9	7.2	2.8	47,800
Device 4	Cs (0 nm) / Au (20 nm)	-	-	-	7.8	-

η_{ext}, η_{PE} and V_{1000} are the values at 1000 cd/m^2, respectively. V_T and L_{max} are the turn-on voltage at a luminance of 0.1 cd/m^2 and the maximum luminance, respectively.

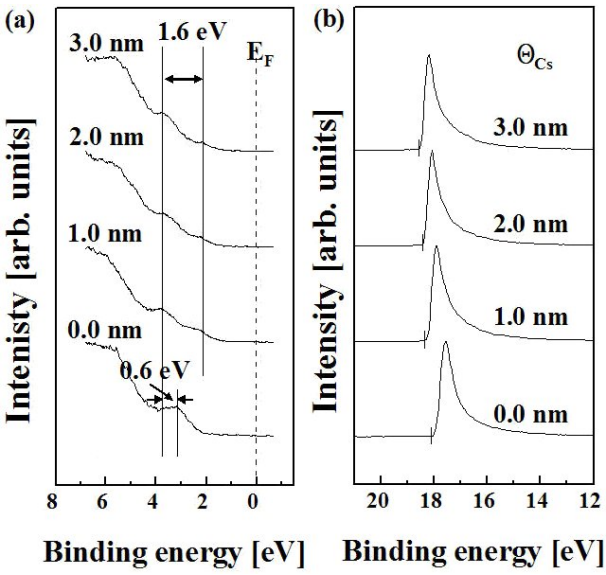

Fig. 2. UPS spectra near (a) the onset and (b) the valence bands as functions of the Cs layer thickness on Alq_3.

vices. Figure 1(b) shows the external quantum efficiency-luminance - power efficiency curves for devices 1-3. As shown in Table 1, the maximum luminance (L_{max}), external quantum efficiency (η_{ext}) at a luminance of 1000 cd/m^2 (L_{1000}) and power efficiency (η_{PE}) at L_{1000} of devices $1 \sim 3$ increased with decreasing Cs thickness from 3 to 1 nm. Device 3 with a 1.0-nm-thick Cs layer, which exhibited a light output of L_{max} = 47800 cd/m^2, η_{ext} = 2.0 % and η_{PE} = 1.9 lm/W, showed the highest device performance compared with the other devices. This device performance could be explained by the efficiency of electron injection into the interface. In addition, the mechanism for electron injection can be understood by analyzing the electronic structures of the interface.

Figure 2(a) shows the spectral region around the highest occupied molecular orbitals (HOMOs) of Alq_3 in the UPS spectra as functions of Θ_{Cs} on Alq_3. All the Alq_3 molecular orbital features were shifted to a higher binding energy, and a new state was formed in the previously forbidden energy gap. The UPS measurements show that while a 1.0 nm thick Cs layer had been deposited onto Alq_3, the spectral features were attenuated. The peaks in the UPS spectra remain as identifiable and were shifted (by a realignment of the molecular levels) to a higher binding energy (by approximately 0.6 eV) compared with the pristine Alq_3. A new state was observed at approximately 1.6 eV above the HOMO of Alq_3. A new gap state has also been observed in several interfaces between a low work function metal (*e.g.*, alkali metal (Li, Na, and K) or alkaline earth metal (Ca and Mg)) and Alq_3 [18]. In the electronic studies by UPS, the low work function metal-induced gap state is important for understanding the interactions between organic materials and metals. These interactions can have a direct influence on the energy barrier for charge carrier injection, and on other important physical processes, such as the quenching of excitations [19].

The most accepted model [7] for efficient electron injection from a metal into an organic layer, such as Alq_3, has been used to examine the Φ_n^B between the metal Fermi level and the lowest unoccupied molecular orbital (LUMO) of an ETL. Figure 2(b) shows the relative difference in the work function (Φ_{Alq_3}-Φ_{Cs/Alq_3}) between the pristine Alq_3 and the Alq_3 / Cs-on-Alq_3 interfaces.

Figure 3 shows the evolution of the proposed energy band diagrams in the interfaces formed, from left to right, with increasing Cs layer thickness on Alq_3. Here, the barrier height for electron injection, Φ_B^N, is given by the following equation:

$$\Phi_B^N = \Phi_{Alq_3} - A - \Delta,$$

where Φ_{Alq_3} is the work function of the pristine 10-nm-thick Alq_3 layer and A is the LUMO energy level of Alq_3 at the Cs-on-Alq_3 interface. Δ is the vacuum level (VL) shift of Φ_{Alq_3}-Φ_{Cs/Alq_3}. The energy band gap (E_g) of pristine Alq_3 was 2.9 eV [7]. When Θ_{Cs} was increased from 1.0 to 3.0 nm on Alq_3, the HOMO level of the interfaces does not change from 2.7 eV below the Fermi

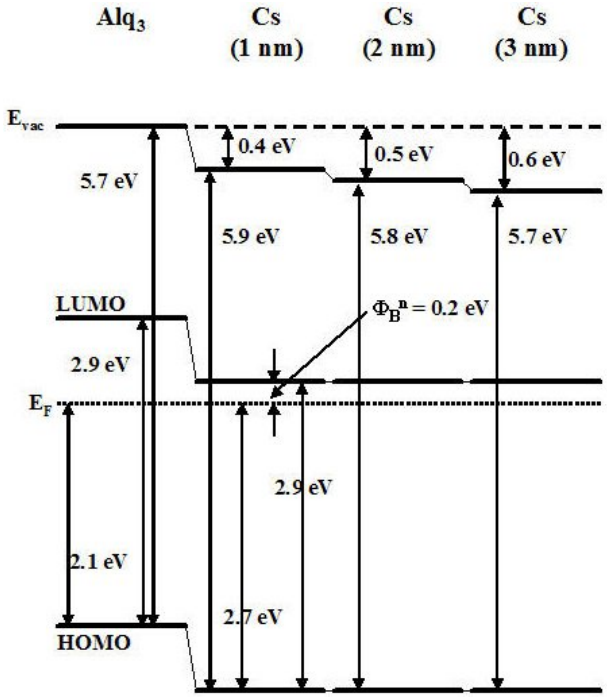

Fig. 3. Evolution of the proposed energy band diagrams, from left to right, with increasing deposition of Cs on Alq_3.

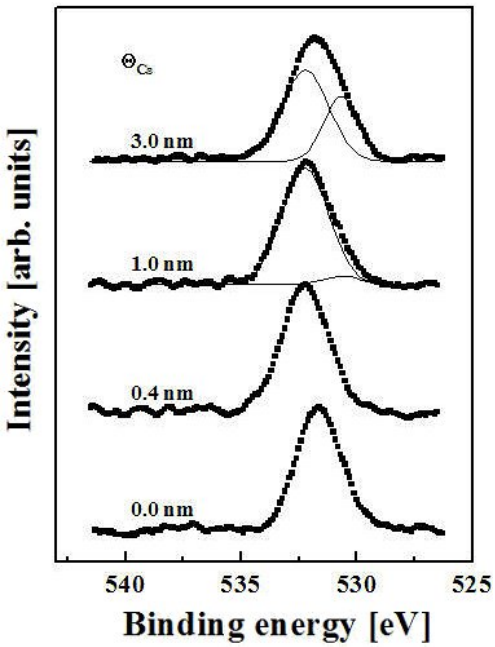

Fig. 4. Evolution of the XPS O 1s core-level electron-density curves as a function of the Cs coverage on Alq_3.

level, but the ionization potential decreases from 5.9 to 5.7 eV. This means that ΦBN of the interface is almost identical, 0.2 eV at Θ_{Cs} ($1 \sim 3$ nm) on Alq_3.

In order to further investigate the interfacial chemical reaction, the O 1s core-level EDCs of the Cs-on-Alq_3 were analyzed by using XPS. Figure 4 shows the evolution of the O 1s EDCs as a function of Θ_{Cs} on Alq_3 (100 Å). For $\Theta_{Cs} = 0$ Å, the O 1s core-level EDC was symmetrical in shape and was composed of a single component, indicating a clean Alq_3 film. The single component of the O 1s EDC shifts initially to a higher binding energy of 532.2 eV (forming a stable Alq_3 radical anion without a decomposition) until $\Theta_{Cs} = 0.4$ nm, compared with the pristine Alq_3 of 531.6 eV. From $\Theta_{Cs} = 1.0$ nm, a O 1s peak of 530.6 eV with low intensity begins to appears at a lower binding energy, and the intensity of the 530 6-eV peak is further increased at $\Theta_{Cs} = 3.0$ nm. The peak shift to a lower binding energy originates from a decrease in the Coulomb potential between the nuclei and the electrons of the valence band [1,9] as a result of the increased electron density at the valence band of O atoms due to the existence of an electron provided by Cs. The peak shift to a lower binding energy of 1.6 eV might cause bond breaking between the Al and the O atoms in the Alq_3 molecule [11]. Therefore, the peak at a low binding energy of 530.6 eV appears to be caused by the appearance of a metallic Alq_3 component that was decomposed by largely electronic charge transfer from Cs for higher coverage.

The energy difference (1.6 eV) between a radical anion and a metallic component in the XPS spectra of the O 1s core level is almost identical to the 1.6 eV observed between the new gap state and the HOMO level. This is consistent with the results reported by Shen *et al.* in the Mg / Alq_3 interfaces [18]. As mentioned above, a staged interface reaction involving two steps, in which a stable radical anion component and a metallic component are formed, was observed when Θ_{Cs} was increased from 0 to 3 nm on Alq_3. As shown in Figure 4, the formation of a stable radical anion at $\Theta_{Cs} = 0.4$ nm leads to a stable device performance of the TEOLED, as shown in Figure 1. However, the appearance of a metallic component at $\Theta_{Cs} \geq 1$ nm results in poor driving of these devices.

IV. CONCLUSIONS

The interfacial electronic features of Cs-on-Alq_3 revealed a relatively unchanged HOMO level at 2.1 eV below Fermi level when Cs from 1 to 3 nm was deposited on Alq_3. However, the ionization potential was decreased from 5.9 to 5.7 eV by the dipole interfaces formed between Cs and Alq_3. The proposed energy band diagram showed that Φ_B^N was 0.2 eV for all devices containing Cs.

The valence band spectra of the Cs-on-Alq_3 interfaces at $\Theta_{Cs} \geq 1$ showed that the HOMO level was shifted downward by 0.6 eV compared with that of the pristine Alq_3. In addition, a new gap state was formed at approximately 1.1 eV below the Fermi level. The difference in this energy level is consistent with the formation of both a radical anion and a metallic component in the O 1s core-level electron-density curves.

An examination of the device performance of the TEOLEDs showed that although Φ_B^N was almost identical, the production of a stable radical anion component at Θ_{Cs} (0.4 nm) allowed efficient electron injection. On the other hand, a metallic component caused by the decomposition of Alq_3 at $\Theta_{Cs} > 1.0$ nm resulted in poor device performance.

ACKNOWLEDGMENTS

This study was supported by the National Program for Tera-level Nanodevices of the Korea Ministry of Science and Technology as a 21st Century Frontier Program and by Pohang Accelerator Laboratory in Korea.

REFERENCES

[1] F. Gutmann and L. E. Lyons, *Organic Semiconductors* (Wiley, New York, 1997).
[2] C. W. Tang and S. A. Vanslyke, Appl. Phys. Lett. **51**, 913 (1987).
[3] J. H. Seo, J. H. Seo, Y. K. Kim, G. W. Hyung, J. H. Kim, K. H. Lee and S. S. Yoon, J. Korean Phys. Soc. **51**, S289 (2007).
[4] H.-Y. Fu, F. Xiao, B.-X. Shao, X.-D. Gao, H.-R. Wu, Y.-Q. Zhan and X. Y. Hou, J. Korean Phys. Soc. **50**, 479 (2007).
[5] C. W. Tang, Appl. Phys. Lett. **48**, 183 (1986).
[6] L. Wang, D. Fine, D. Sharma, L. Torsi and A. Dodabalapur, Anal. Bioanal. Chem. **384**, 310 (2006).
[7] H. Ishii, K. Sugiyama, E. Ito and K. Seki, Adv. Mater. **11**, 605 (1999).
[8] K.-Y. Wu, Y.-T. Tao and H.-W. Huang, Appl. Phys. Lett. **99**, 241104 (2007).
[9] V.-E. Choong, M. G. Mason, C. W. Tang and Y. Gao, Appl. Phys. Lett. **72**, 2689 (1998).
[10] G. Parthasarathy, P. E. Burrows, V. Khalfin, V. G. Kozlov and S. R. Forrest, Appl. Phys. Lett. **72**, 2138 (1998).
[11] S. L. Lai, M. K. Fung, S. N. Bao, S. W. Tong, M. Y. Chan, C. S. Lee and S. T. Lee, Chem. Phys. Lett. **367**, 753 (2003).
[12] V. Bulovic, G. Gu, D. E. Burrows, M. E. Thompson and S. R. Forrest, Nature (London) **380**, 29 (1996).
[13] M.-H. Lu, M. S. Weaver, T. X. Zhou, M. Rothman, R. C. Kwong, M. Hack and J. J. Brown, Appl. Phys. Lett. **81**, 3921 (2002).
[14] G. Parthasarathy, C. Adachi, P. E. Burrows and S. R. Forrest, Appl. Phys. Lett. **76**, 2128 (2000).
[15] C.-W. Chen, P.-Y. Hsieh, H.-H. Chiang, C.-L. Lin, H.-M. Wu and C.-C. Wu, Appl. Phys. Lett. **83**, 5127 (2003).
[16] L. S. Hung, C. W. Tang, M. G. Mason, P. Raychaudhuri and J. Madathil, Appl. Phys. Lett. **78**, 544 (2001).
[17] M.-H. Lu and J. C. Sturn, J. Appl. Phys. **91**, 595 (2002).
[18] C. Shen, I. G. Hill, A. Kahn and I. Schwartz, J. Am. Chem. Soc. **122**, 5391 (2000).
[19] N. Johansson, T. Osada, S. Stafström, W. R. Salaneck, V. Parente, D. A. dos Santos, X. Crispin and J. L. Brédas, J. Chem. Phys. **111**, 2157 (1999).